2005 American Control Conference
June 8-10, 2005. Portland, OR, USA

Input-Output Linearization of an Automobile Model With 2-D LuGre Friction

Matthew G. Villella and David G. Taylor
School of Electrical and Computer Engineering
Georgia Institute of Technology
Atlanta, GA 30332

Abstract— **An automobile model is developed through application of LuGre friction. The two-dimensional LuGre friction model is extended to account for an effect of rotational motion. An algebraic solution for normal force distribution is described, eliminating the need for a dynamic suspension model. The relative velocity norm is approximated to produce a sufficiently smooth design model for Input-Output Linearization. Relative degree is evaluated and singularities lead to reduction from three to two outputs. Well defined relative degree for the two output case is shown to require small friction forces. A control design is presented as well as the zero dynamics of the system. Finally, the controller is simulated and results are presented.**

I. Introduction

Automobiles are difficult, if not impossible, for a driver to control on a slippery road. This problem has led automobile manufacturers to develop a wide range of electronic systems to improve vehicle response to the driver [1].

The first of such systems were Antilock Braking Systems (ABS) which attempt to reduce wheel slip during braking. ABS was followed by Traction Control Systems (TCS) and Vehicle Stability Control Systems (VSC) in rapid succession. These systems apply braking force to a vehicle's wheels to limit slip during vehicle acceleration and to respond more effectively to driver steering commands in adverse situations, respectively.

Complementing these advances in automobile braking system technology have been proliferations in designs of All-Wheel-Drive (AWD) systems. Such systems mechanically transmit engine drive torque to all of the vehicle wheels in varying ratios. In addition, electronically controllable AWD systems that provide active means for transfer of torque to individual wheels have become available. Paralleling this mechanical technology is the implementation of electric vehicle concepts which have individual motors powering each wheel, allowing for independent, fast torque generation at each vehicle corner.

These developments motivate consideration of how to best apply torque to wheels to achieve vehicle dynamic objectives with the aim of assisting the driver to maintain authority over the motion of the automobile.

Numerous authors have presented control designs developed through a variety of standard techniques (e.g., [2],[3]). However, the majority of the previous automobile control work has relied upon empirical friction models, such as the well known Pacjeka model of [4].

Empirical friction models consist of fits to steady-state measurements and are thus unable to predict physical effects not observed in the data. They are limited both by the data that are available and by the measurement methods. They also assume a fixed functional form which is typically chosen by ad hoc means and is not related to the underlying physics.

The limitations of empirical friction models have motivated the development of a class of first-principles dynamic friction models. Among these is the LuGre model, which was first presented in [5] and subsequently applied to the automobile modeling problem in [6],[7],[8].

In the following, the LuGre model shall be the basis for the development of a vehicle model for Input-Output Linearization (IOL) control design. An extension to the LuGre model which is necessary to model combined translational and rotational vehicle motion is developed. An algebraic solution for normal force variation due to load transfer is presented. The vehicle dynamics, friction, and normal force models are then assembled into the complete vehicle model.

Using the vehicle model, a controller is designed for combined longitudinal velocity and yaw rate control of the vehicle via IOL. Relative degree for the system is analyzed and a method for avoiding a singularity in the computation of the control is discussed. The zero dynamics of the controlled system are considered. Finally, the control is simulated and the results are presented and discussed.

II. Vehicle Model

A. Vehicle Motion Dynamics

The dynamical equations for an automobile moving in a plane, derived from Newton's Laws may be written as

$$m\dot{v}_x = \sum_{i=1}^{4} \left(F_{x,i}\cos\theta_i - F_{y,i}\sin\theta_i\right) + m\omega_v v_y \quad (1a)$$

$$m\dot{v}_y = \sum_{i=1}^{4} \left(F_{x,i}\sin\theta_i + F_{y,i}\cos\theta_i\right) - m\omega_v v_x \quad (1b)$$

$$I\dot{\omega}_v = \sum_{i=1}^{4} \left(x_i\sin\theta_i - y_i\cos\theta_i\right) F_{x,i} + \sum_{i=1}^{4} \left(x_i\cos\theta_i + y_i\sin\theta_i\right) F_{y,i} \quad (1c)$$

0-7803-9098-9/05/$25.00 ©2005 AACC

where v_x and v_y are the forward and lateral velocities, respectively, ω_v is the angular velocity or yaw rate of the vehicle, m is the vehicle mass, I is the vehicle inertia, $F_{x,i}$ and $F_{y,i}$ are the longitudinal and lateral forces applied to the ith wheel, θ_i is the steer angle of the ith wheel, and x_i, y_i are the longitudinal and lateral moment arms of the ith wheel with respect to the vehicle center of gravity. The order in which the wheels are indexed is inconsequential as long as the chosen ordering convention is employed consistently throughout. Note that (1) may be employed for vehicles with an arbitrary number of wheels by adjusting the summation indices accordingly.

Similarly, the dynamical equations for the wheel rotation may be written as

$$I_w \dot{\omega}_{w,i} = r F_{x,i} + \tau_i \tag{2}$$

where $\omega_{w,i}$ is the rotational velocity of the ith wheel, I_w and r are the scalar wheel inertia and wheel radius, respectively, which are assumed to be identical for all wheels, and τ_i is the input torque applied to the ith wheel. A right-handed coordinate convention has been employed, resulting in a positive sign for *backwards* wheel rotation.

B. LuGre Friction

Equations (1) and (2) are incomplete, however, since the way in which the force vectors arise has not yet been addressed. These forces result from the frictional contact of the wheel and the road surface and many models have been proposed to describe the phenomenon of friction. The LuGre model, however, which was originally proposed in [5], is among a class of models that provides a first principles physical interpretation of friction as the interaction of surface asperities at the contact interface, which may be treated as deformable bristles. The dynamics of these bristles were extended to two dimensions in [8] as[1]

$$\dot{\zeta}_x = -v_{r,x} - \frac{\sigma_{0,x}\|\boldsymbol{v}_r\|}{\Gamma(\boldsymbol{v}_r)}\zeta_x \tag{3a}$$

$$\dot{\zeta}_y = -v_{r,y} - \frac{\sigma_{0,y}\|\boldsymbol{v}_r\|}{\Gamma(\boldsymbol{v}_r)}\zeta_y \tag{3b}$$

where ζ_x, ζ_y are the bristle deflection length components, $v_{r,x}$, $v_{r,y}$ are components of the relative velocity between the wheel and road at the contact point, $\sigma_{0,x}, \sigma_{0,y}$ are stiffness constants along each axis, and $\boldsymbol{v}_r = [v_{r,x}, v_{r,y}]^T$ is the vector relative velocity. Furthermore, the function $\Gamma(\boldsymbol{v}_r)$ is defined as

$$\Gamma(\boldsymbol{v}_r) = \mu_d + (\mu_s - \mu_d)e^{-\|\boldsymbol{v}_r\|^\alpha / v_s^\alpha} \tag{4}$$

where μ_s and μ_d are static and dynamic Coulomb friction coefficients, v_s is the Stribeck velocity, and α is a shape parameter that influences the speed of transition from static to dynamic friction.

[1]The equation is given here with an opposite sign convention for v_r from [8].

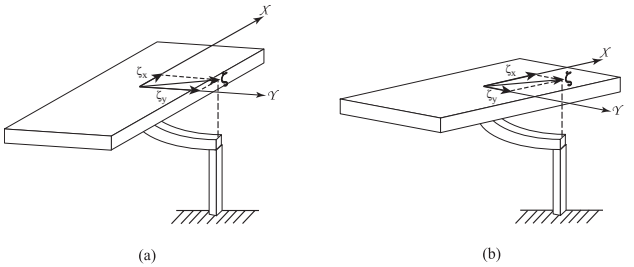

Fig. 1. Deflection of a bristle attached to a rotating body (a) before and (b) after the body rotation.

The model of (3a)-(3b) provides an accurate physical description of bristle deflection for 2-D translational motion, however, it neglects an important effect produced by combined translational and rotational motion. Namely, the explicit coupling of the bristle deflection dynamics of the two axes due to rotation of the body-fixed coordinate frame in which bristle deflections are measured.

This effect is illustrated in Figure 1, which shows a bristle, attached to a body and in contact with a fixed surface asperity, before and after a body rotation. While the deflection of the bristle remains fixed with respect to the surface asperity, the bristle deflection vector is rotated with respect to the body-fixed frame.

Mathematically, this effect is accounted for by writing the total rate of change of the bristle deflection vector, $\boldsymbol{\zeta} = [\zeta_x, \zeta_y]^T$, as (see, e.g. [9])

$$\frac{d\boldsymbol{\zeta}}{dt} = \frac{\partial \boldsymbol{\zeta}}{\partial t} + \boldsymbol{\omega} \times \boldsymbol{\zeta} \tag{5}$$

where $\boldsymbol{\omega}$ is the angular velocity vector of the coordinate frame in which the bristle deflection is measured. It is multiplied with the bristle deflection vector, using the vector cross product, to give the rate of change of the bristle deflection vector due to the coordinate frame rotation. The partial derivative of the deflection vector with respect to time gives the instantaneous time rate of change of the vector due to bristle motion with respect to the coordinate frame, which is simply the vector of component-wise time derivatives.

Addition of the rotational effect results in the revision of (3a)-(3b) as

$$\dot{\zeta}_x = -v_{r,x} - \frac{\sigma_{0,x}\|\boldsymbol{v}_r\|}{\Gamma(\boldsymbol{v}_r)}\zeta_x + \omega_z\zeta_y \tag{6a}$$

$$\dot{\zeta}_y = -v_{r,y} - \frac{\sigma_{0,y}\|\boldsymbol{v}_r\|}{\Gamma(\boldsymbol{v}_r)}\zeta_y - \omega_z\zeta_x \tag{6b}$$

where ω_z is the angular velocity about the z-axis, which is the sole angular velocity component.

The LuGre output equations which give the x and y components of the force applied to the wheel by the road as a result of frictional contact are

$$F_x \equiv \mu_x N = \Big[\sigma_{0,x}\zeta_x + \sigma_{1,x}(\dot{\zeta}_x - \omega_z\zeta_y) - \sigma_{2,x}v_{r,x}\Big]\, N \tag{7a}$$

$$F_y \equiv \mu_y N = \Big[\sigma_{0,y}\zeta_y + \sigma_{1,y}(\dot{\zeta}_y + \omega_z\zeta_x) - \sigma_{2,y}v_{r,y}\Big]\, N \tag{7b}$$

where μ_x, μ_y are friction coefficient functions, N is the normal force applied by the road to the wheel, $\sigma_{1,x}, \sigma_{1,y}$ are damping coefficients, and $\sigma_{2,x}, \sigma_{2,y}$ are viscous damping coefficients. This differs from the output equations of [8] due to the redefinition of $\dot{\zeta}_x$ and $\dot{\zeta}_y$.

C. Normal Force

While (7) defines the forces applied to each wheel for use in (1) and (2), the normal forces exerted on each wheel are, as yet, unknown. There are two possibilities for determination of the normal forces. The first is to utilize a dynamic suspension model, with springs and dampers that apply force to the wheels as a function of vehicle body pitch and roll. Alternatively, the normal forces may be solved for by means of a static force and moment balance analysis. While this second method results in a less complex model, the solution of the static force and moment balance for the vehicle is indeterminate since only three equations are available in four normal force unknowns.

One solution for utilizing the static force and moment balance in spite of the indeterminate nature of the problem is presented in [10] and employs a hypothetical suspension model in which the spring stiffnesses of the suspension model are allowed to approach infinity. This results in the algebraic solution

$$\boldsymbol{N} = mg\boldsymbol{L}\left(\boldsymbol{L}^T\boldsymbol{L} + h\boldsymbol{P}\boldsymbol{L}\right)^{-1}\boldsymbol{u}_3 \tag{8}$$

where $\boldsymbol{N} = [N_1, \ldots, N_4]^T$ are the ordered normal forces at each wheel, g is the gravitational constant, h is the height of the vehicle center of gravity above the ground, $\boldsymbol{u}_3 = [0, 0, 1]^T$ is a unit vector,

$$\boldsymbol{L} = \begin{bmatrix} x_1 & y_1 & 1 \\ \vdots & \vdots & \vdots \\ x_4 & y_4 & 1 \end{bmatrix} \tag{9}$$

is a constant matrix, and the ith column of the matrix $\boldsymbol{P}$ is

$$\{\boldsymbol{P}\}_i = \begin{bmatrix} \cos\theta_i \\ \sin\theta_i \\ 0 \end{bmatrix}\mu_{x,i} + \begin{bmatrix} -\sin\theta_i \\ \cos\theta_i \\ 0 \end{bmatrix}\mu_{y,i} \tag{10}$$

for $i = 1, \ldots, 4$, where $\mu_{x,i}$ and $\mu_{y,i}$ are the force coefficients of (7) for the ith wheel.

The matrix inverse in (8) exists at least locally in a neighborhood of the equilibrium $\boldsymbol{P} \equiv 0$ as long as $\boldsymbol{L}^T\boldsymbol{L}$ is invertible.

D. Vehicle Model Summary

Defining state vector partitions, $\boldsymbol{\xi} = [v_x, v_y, \omega_v]^T$ and $\boldsymbol{\nu} = [\omega_{w,1}, \ldots, \omega_{w,4}]^T$, (1), (2), and (7) may be written concisely as

$$\boldsymbol{M}\dot{\boldsymbol{\xi}} = \boldsymbol{A}\boldsymbol{N} + \boldsymbol{\eta}(\boldsymbol{\xi}) \tag{11}$$

$$I_w\dot{\boldsymbol{\nu}} = r\boldsymbol{\mu}_x\boldsymbol{N} + \boldsymbol{\tau} \tag{12}$$

where $\boldsymbol{M} = \mathrm{diag}(m, m, I)$, $\boldsymbol{\mu}_x = \mathrm{diag}(\mu_{x,1}, \ldots, \mu_{x,4})$, $\boldsymbol{\tau} = [\tau_1, \ldots, \tau_4]^T$, $\boldsymbol{N}$ is as defined in (8), the ith column of the matrix $\boldsymbol{A}$ is defined as

$$\{\boldsymbol{A}\}_i = \begin{bmatrix} \cos\theta_i \\ \sin\theta_i \\ x_i\sin\theta_i - y_i\cos\theta_i \end{bmatrix}\mu_{x,i} + \begin{bmatrix} -\sin\theta_i \\ \cos\theta_i \\ x_i\cos\theta_i + y_i\sin\theta_i \end{bmatrix}\mu_{y,i} \tag{13}$$

for $i = 1, \ldots, 4$, and

$$\boldsymbol{\eta}(\boldsymbol{\xi}) = m\omega_v[v_y, -v_x, 0]^T = m\xi_3[\xi_2, -\xi_1, 0]^T \tag{14}$$

In addition, four sets of the bristle deflection dynamical equations of (6) are required – one for each wheel – and, assuming identical bristle characteristics for the four wheels, may be written in matrix-vector form as

$$\dot{\boldsymbol{\zeta}}_x = -\boldsymbol{v}_{r,x} - \sigma_{0,x}\boldsymbol{V}\boldsymbol{\zeta}_x + \boldsymbol{W}\boldsymbol{\zeta}_y \tag{15a}$$

$$\dot{\boldsymbol{\zeta}}_y = -\boldsymbol{v}_{r,y} - \sigma_{0,y}\boldsymbol{V}\boldsymbol{\zeta}_y - \boldsymbol{W}\boldsymbol{\zeta}_x \tag{15b}$$

where $\boldsymbol{\zeta}_x, \boldsymbol{\zeta}_y$ are ordered vectors of x and y bristle deflection, $\boldsymbol{v}_{r,x}, \boldsymbol{v}_{r,y}$ are ordered vectors of x and y relative velocity,

$$\boldsymbol{V} = \mathrm{diag}\left(\frac{\|\boldsymbol{v}_{r,1}\|}{\Gamma(\boldsymbol{v}_{r,1})}, \ldots, \frac{\|\boldsymbol{v}_{r,4}\|}{\Gamma(\boldsymbol{v}_{r,4})}\right) \tag{16}$$

where $\boldsymbol{v}_r$ is subscripted to indicate the corresponding wheel,

$$\boldsymbol{W} = \left(\omega_v\boldsymbol{I} + \mathrm{diag}(\dot{\boldsymbol{\theta}})\right) \tag{17}$$

where $\boldsymbol{I}$ is the identity matrix, and $\boldsymbol{\theta}$ is a vector of ordered steer angles.

Finally, the relative velocities at each wheel-road interface are implicitly required in (11)-(12), and explicitly required in (15). These velocities are given by

$$v_{r,x,i} = [\cos\theta_i, \sin\theta_i, x_i\sin\theta_i - y_i\cos\theta_i]\boldsymbol{\xi} + r\nu_i \tag{18a}$$

$$v_{r,y,i} = [-\sin\theta_i, \cos\theta_i, x_i\cos\theta_i + y_i\sin\theta_i]\boldsymbol{\xi} \tag{18b}$$

which comes from the kinematics of the vehicle motion.

III. Vehicle Control

The control objective is to track an arbitrary velocity trajectory for motion in the two-dimensional plane. Such motion is fully described by three variables: longitudinal, lateral, and angular velocity. Functions of these velocities may thus be specified as the system output, depending on specific vehicle motion control objectives. Assuming that wheel torque at all four wheels may be independently specified, the system has four inputs and up to three independent outputs.

Some simplifying assumptions are employed, making the control development in some sense ideal and thus an indication of the best possible control that may be achieved. Ideal torque sources are assumed at each wheel, which provide positive and negative torque, and may be adjusted arbitrarily fast. Static and dynamic coefficients of

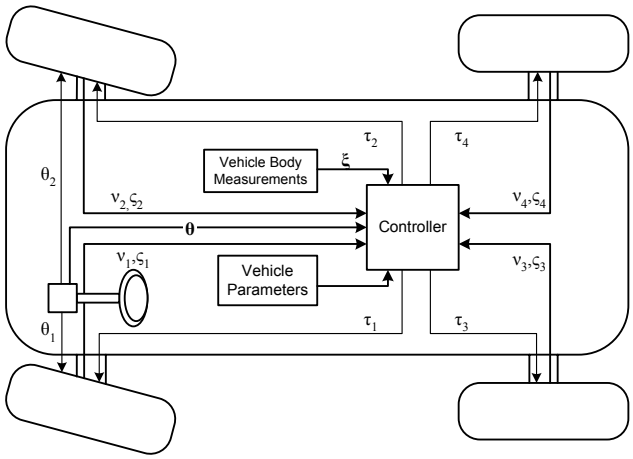

Fig. 2. Vehicle control architecture.

TABLE I
MODEL PARAMETERS.

Parameter	Value	Units
m	907.2	kg
I	514.1	kg m^2
I_w	0.136	kg m^2
r	0.2	m
h	0.5	m
x_F (front)	1	m
x_R (rear)	-1.2	m
y_L (left)	-0.7	m
y_R (right)	0.7	m
μ_s	0.2	-
μ_d	0.1	-
α	0.5	-
v_s	5.5	m/s
$\sigma_{0,x}, \sigma_{0,y}$	178	m^{-1}
$\sigma_{1,x}, \sigma_{1,y}$	1	s/m
$\sigma_{2,x}, \sigma_{2,y}$	0	s/m

friction between the wheels and road are considered to be constant, known parameters. Similarly, measurements of all system states are assumed to be available, including bristle deflections.

In actuality, friction coefficients vary and are not well known, and full state measurements are typically not available. Thus, practical applications would require both parameter and state estimation techniques to be employed.

A block diagram of the control architecture is shown in Figure 2. The rear wheels are fixed at zero steer angle and the front wheels are constrained to steer so that the angular rotation axes of all four wheels intersect at a single point. Thus, specifying the steer angle for one front wheel uniquely determines the steer angle of the other wheel.

The driver generates the time-varying exogenous steering signal for the left wheel, which is fed into the controller. Measurements of the velocities and bristle deflections are also input to the controller. The controller has access to the pre-defined parameters, listed in Table I, including system masses and inertias, bristle stiffnesses, and coefficients of friction. Front and rear as well as left and right moment arms are chosen to be equal for vehicle symmetry. Finally, the controller outputs torque to the wheels.

A. Design Model

A necessary condition for employing IOL is that the design model be sufficiently smooth such that all derivatives that must be computed exist and are continuous. However, in the case of the friction model of (15), the smoothness condition is not met due to the appearance of the relative velocity norms which have discontinuous derivatives at $\boldsymbol{v}_r = 0$.

This difficulty may be avoided by employing a polynomial estimate in a neighborhood of zero relative velocity. This estimate is

$$\|\boldsymbol{v}_r\|^* = -\frac{v_{r,x}^4}{8\rho^3} - \frac{v_{r,y}^4}{8\rho^3} + \frac{3v_{r,x}^2}{4\rho} + \frac{3v_{r,y}^2}{4\rho} - \frac{v_{r,y}^2 v_{r,x}^2}{4\rho^3} + \frac{3\rho}{8} \quad (19)$$

where ρ is a small parameter, but large enough to avoid numerical computation difficulties. A choice of $\rho = 10^{-4}$ has been observed to work well. Then the approximate relative velocity norm is

$$\widehat{\|\boldsymbol{v}_r\|} = \begin{cases} \|\boldsymbol{v}_r\|^*, & \|\boldsymbol{v}_r\| \le \rho \\ \|\boldsymbol{v}_r\|, & \|\boldsymbol{v}_r\| > \rho \end{cases} \quad (20)$$

which is substituted into (16) in place of $\|\boldsymbol{v}_r\|$.

B. Relative Degree

In order to design an IOL controller, it is necessary to first determine the relative degree of the system. Since the vehicle body velocities fully describe the motion of the vehicle, the output is tentatively selected as $\boldsymbol{\xi}$.

Differentiating $\boldsymbol{\xi}$ until the input, $\boldsymbol{\tau}$, appears yields

$$\begin{aligned} \boldsymbol{M}\ddot{\boldsymbol{\xi}} = &\left(\frac{\partial(\boldsymbol{AN})}{\partial\boldsymbol{\xi}} + \frac{\partial\boldsymbol{\eta}(\boldsymbol{\xi})}{\partial\boldsymbol{\xi}}\right)\dot{\boldsymbol{\xi}} + \frac{\partial(\boldsymbol{AN})}{\partial\boldsymbol{\nu}}\dot{\boldsymbol{\nu}} \\ &+ \frac{\partial(\boldsymbol{AN})}{\partial\boldsymbol{\zeta}_x}\dot{\boldsymbol{\zeta}}_x + \frac{\partial(\boldsymbol{AN})}{\partial\boldsymbol{\zeta}_y}\dot{\boldsymbol{\zeta}}_y + \frac{\partial(\boldsymbol{AN})}{\partial\boldsymbol{\theta}}\dot{\boldsymbol{\theta}} \end{aligned} \quad (21)$$

and substituting $\dot{\boldsymbol{\nu}}$ from (12) into (21), the result may be written as

$$\boldsymbol{M}\ddot{\boldsymbol{\xi}} = \boldsymbol{f}(\boldsymbol{\xi}, \boldsymbol{\nu}, \boldsymbol{\zeta}) + \boldsymbol{G}(\boldsymbol{\xi}, \boldsymbol{\nu}, \boldsymbol{\zeta})\boldsymbol{\tau} \quad (22)$$

where

$$\begin{aligned} \boldsymbol{f}(\boldsymbol{\xi}, \boldsymbol{\nu}, \boldsymbol{\zeta}) = &\left(\frac{\partial(\boldsymbol{AN})}{\partial\boldsymbol{\xi}} + \frac{\partial\boldsymbol{\eta}(\boldsymbol{\xi})}{\partial\boldsymbol{\xi}}\right)\dot{\boldsymbol{\xi}} \\ &+ \frac{r}{I_w}\frac{\partial(\boldsymbol{AN})}{\partial\boldsymbol{\nu}}\boldsymbol{\mu}_x\boldsymbol{N} + \frac{\partial(\boldsymbol{AN})}{\partial\boldsymbol{\theta}}\dot{\boldsymbol{\theta}} \\ &+ \frac{\partial(\boldsymbol{AN})}{\partial\boldsymbol{\zeta}_x}\dot{\boldsymbol{\zeta}}_x + \frac{\partial(\boldsymbol{AN})}{\partial\boldsymbol{\zeta}_y}\dot{\boldsymbol{\zeta}}_y \end{aligned} \quad (23)$$

with $\dot{\boldsymbol{\xi}}, \dot{\boldsymbol{\zeta}}_x, \dot{\boldsymbol{\zeta}}_y$ found from (11) and (15), and the decoupling matrix is

$$\boldsymbol{G}(\boldsymbol{\xi}, \boldsymbol{\nu}, \boldsymbol{\zeta}) = \frac{1}{I_w}\frac{\partial(\boldsymbol{AN})}{\partial\boldsymbol{\nu}} \quad (24)$$

From (22), the system appears to have relative degree $[2, 2, 2]$, but this is only the case if the decoupling matrix has

full row rank so that the existence of at least one solution for $\boldsymbol{\tau}$ is guaranteed. Therefore, expanding the partial derivative in (24),

$$\begin{aligned}\boldsymbol{G}(\boldsymbol{\xi},\boldsymbol{\nu},\boldsymbol{\zeta})=&\frac{1}{I_w}\frac{\partial(\boldsymbol{AN})}{\partial \boldsymbol{v}_{r,x}}\frac{\partial \boldsymbol{v}_{r,x}}{\partial \boldsymbol{\nu}}\\ =&\frac{r}{I_w}\left(\boldsymbol{R}_x\frac{\partial \boldsymbol{\mu}_x}{\partial \boldsymbol{v}_{r,x}}+\boldsymbol{R}_y\frac{\partial \boldsymbol{\mu}_y}{\partial \boldsymbol{v}_{r,x}}\right)\mathrm{diag}(\boldsymbol{N})\end{aligned} \quad (25)$$

since $\partial \boldsymbol{v}_{r,x}/\partial \boldsymbol{\nu}=r\boldsymbol{I}$ from (18a) and where

$$\boldsymbol{R}_x=\left(\boldsymbol{A}_x+h\boldsymbol{AL}(\boldsymbol{L}^T\boldsymbol{L}+h\boldsymbol{PL})^{-1}\boldsymbol{P}_x\right) \quad (26a)$$

$$\boldsymbol{R}_y=\left(\boldsymbol{A}_y+h\boldsymbol{AL}(\boldsymbol{L}^T\boldsymbol{L}+h\boldsymbol{PL})^{-1}\boldsymbol{P}_y\right) \quad (26b)$$

where $\boldsymbol{P}_x, \boldsymbol{P}_y$ and $\boldsymbol{A}_x, \boldsymbol{A}_y$ are the coefficient matrices of $\boldsymbol{\mu}_x$ and $\boldsymbol{\mu}_y$ from (10) and (13), respectively.

Furthermore, the friction output function derivatives are

$$\frac{\partial \boldsymbol{\mu}_x}{\partial \boldsymbol{v}_{r,x}}=-\sigma_{0,x}\sigma_{1,x}\frac{\partial \boldsymbol{V}}{\partial \boldsymbol{v}_{r,x}}\mathrm{diag}(\boldsymbol{\zeta}_x)-(\sigma_{2,x}+\sigma_{1,x})\boldsymbol{I} \quad (27a)$$

$$\frac{\partial \boldsymbol{\mu}_y}{\partial \boldsymbol{v}_{r,x}}=-\sigma_{0,y}\sigma_{1,y}\frac{\partial \boldsymbol{V}}{\partial \boldsymbol{v}_{r,x}}\mathrm{diag}(\boldsymbol{\zeta}_y) \quad (27b)$$

where $\boldsymbol{V}$ is from (15).

The rank of $\boldsymbol{G}(\boldsymbol{\xi},\boldsymbol{\nu},\boldsymbol{\zeta})$ is difficult to assess in closed form, but for sufficiently small $\boldsymbol{\mu}_x$, $\boldsymbol{\mu}_y$, the decoupling matrix is approximately

$$\boldsymbol{G}(\boldsymbol{\xi},\boldsymbol{\nu},\boldsymbol{\zeta})\approx\frac{r}{I_w}\left(\boldsymbol{A}_x\frac{\partial \boldsymbol{\mu}_x}{\partial \boldsymbol{v}_{r,x}}+\boldsymbol{A}_y\frac{\partial \boldsymbol{\mu}_y}{\partial \boldsymbol{v}_{r,x}}\right)\mathrm{diag}(\boldsymbol{N}) \quad (28)$$

and in the particular case of straight-line motion where $\boldsymbol{\zeta}_y=0, \boldsymbol{\theta}=0$, the matrix does not have full row rank since its second row is identically zero, resulting in a relative degree singularity.

Thus, the system does not have well defined relative degree when lateral velocity is an output. However, selecting only longitudinal and angular velocity as outputs, the reduced decoupling matrix consists of the first and third rows of $\boldsymbol{G}(\boldsymbol{\xi},\boldsymbol{\nu},\boldsymbol{\zeta})$, and maintains full row rank as long as $\partial \boldsymbol{\mu}_x/\partial \boldsymbol{v}_{r,x}\neq 0$.

Since $\partial \boldsymbol{V}/\partial \boldsymbol{v}_{r,x}$ and $\boldsymbol{\zeta}$ typically have opposite signs, this condition is met as long as $\boldsymbol{v}_{r,x}$ and $\boldsymbol{\zeta}_x$ remain small such that, from (27a),

$$-\frac{\partial \boldsymbol{V}}{\partial \boldsymbol{v}_{r,x}}\mathrm{diag}(\boldsymbol{\zeta}_x)<\frac{\sigma_{2,x}+\sigma_{1,x}}{\sigma_{0,x}\sigma_{1,x}}\boldsymbol{I} \quad (29)$$

This bound implies that the friction forces must be kept small in order to maintain relative degree.

When the condition in (29) is met, (22) becomes

$$\boldsymbol{M}_y\ddot{\boldsymbol{y}}=\boldsymbol{f}(\boldsymbol{\xi},\boldsymbol{\nu},\boldsymbol{\zeta})_{1,3}+\boldsymbol{G}(\boldsymbol{\xi},\boldsymbol{\nu},\boldsymbol{\zeta})_{1,3}\boldsymbol{\tau} \quad (30)$$

for the reduced set of outputs, where the subscripts on $\boldsymbol{f}$ and $\boldsymbol{G}$ indicate selection of the first and third rows, $\boldsymbol{M}_y=\mathrm{diag}(m,I)$, and $\boldsymbol{y}=[\xi_1,\xi_3]^T$.

C. Input-Output Linearization

Despite the fact that forces must be kept small in order for the system to have relative degree, control is still possible for less aggressive maneuvers.

The required wheel torque for IOL is computed from (30), using the right pseudo-inverse, to obtain the minimum norm solution as

$$\boldsymbol{\tau}=\boldsymbol{G}_{1,3}^T\left(\boldsymbol{G}_{1,3}\boldsymbol{G}_{1,3}^T\right)^{-1}\left[\boldsymbol{M}_y\ddot{\boldsymbol{y}}_r-\boldsymbol{f}_{1,3}\right] \quad (31)$$

and the vector $\ddot{\boldsymbol{y}}_r$ is defined so as to prescribe second order dynamics as

$$\ddot{\boldsymbol{y}}_r=\ddot{\boldsymbol{y}}^d+\boldsymbol{K}_d(\dot{\boldsymbol{y}}^d-\dot{\boldsymbol{y}})+\boldsymbol{K}_p(\boldsymbol{y}^d-\boldsymbol{y}) \quad (32)$$

where $\boldsymbol{K}_d$ and $\boldsymbol{K}_p$ are positive definite diagonal gain matrices, and $\boldsymbol{y}^d$ is the vector of desired longitudinal and angular velocity outputs. The derivative of $\boldsymbol{y}$ is vehicle longitudinal and yaw acceleration, which may be either measured or computed.

D. Zero Dynamics

With longitudinal and angular velocity outputs, the system has free modes which give rise to zero dynamics. The zero dynamics are found by using $\boldsymbol{y}\equiv\boldsymbol{y}^d$ in (31)-(32), resulting in

$$\boldsymbol{\tau}=-\boldsymbol{G}_{1,3}^T\left(\boldsymbol{G}_{1,3}\boldsymbol{G}_{1,3}^T\right)^{-1}\boldsymbol{f}_{1,3} \quad (33)$$

which is substituted into (11)-(12), producing

$$m\dot{\xi}_2=\boldsymbol{A}_2\boldsymbol{N}-m\xi_1\xi_3 \quad (34a)$$

$$I_w\dot{\boldsymbol{\nu}}=r\boldsymbol{\mu}_x\boldsymbol{N}-\boldsymbol{G}_{1,3}^T\left(\boldsymbol{G}_{1,3}\boldsymbol{G}_{1,3}^T\right)^{-1}\boldsymbol{f}_{1,3} \quad (34b)$$

for any constant ξ_1, ξ_3, where $\boldsymbol{A}_2$ is the second row of $\boldsymbol{A}$. These, combined with the constraint equation

$$0=\boldsymbol{A}_{1,3}\boldsymbol{N}+\boldsymbol{\eta}_{1,3}(\boldsymbol{\xi}) \quad (35)$$

where the subscript on $\boldsymbol{\eta}$ indicates selection of the first and third rows, along with (15), constitute the zero dynamics.

The stability of these zero dynamics is difficult to analyze in closed form. Therefore, the control of (31) is employed in simulation and internal stability is assumed as long as $\boldsymbol{\zeta}_x$, $\boldsymbol{\zeta}_y$, $\boldsymbol{\nu}$, and ξ_2 remain bounded.

IV. Simulation Results

The control is simulated for a lane change maneuver on a slick surface, with the exact relative velocity norm employed in the plant. The steering inputs are piecewise cubic splines. A constant longitudinal acceleration, $\dot{\xi}_1^d=0.2$ m/s^2, is commanded, with an initial velocity of 15 m/s.

The desired angular velocity is specified by solving (18b) under no lateral wheel slip, which provides only two independent equations due to the imposed steering constraints. This allows for elimination of ξ_2, and taking a fraction of the solution for ξ_3, results in

$$\xi_3^d=k_\omega\frac{\xi_1^d\sin\theta}{y_L\sin\theta+(x_\mathrm{F}-x_\mathrm{R})\cos\theta} \quad (36)$$

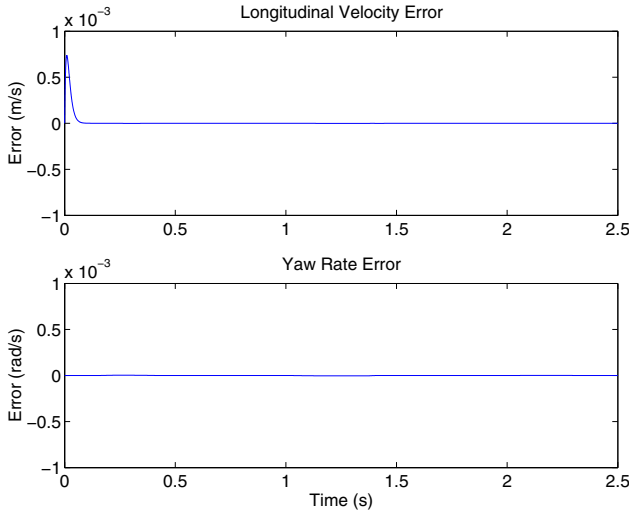

Fig. 3. Error evolution for combined speed and yaw rate control.

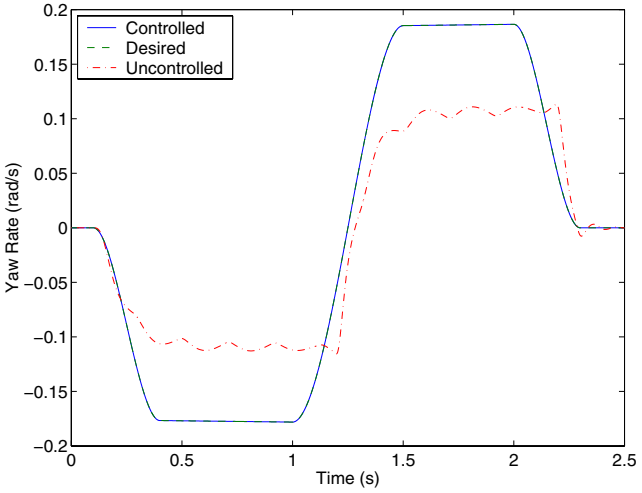

Fig. 4. Comparison of controlled yaw rate response to uncontrolled vehicle response and desired yaw rate.

where k_ω is a scale parameter, and θ is the left-front steer angle. This signal is shown for the lane-change maneuver as the dashed line in Figure 4. The derivatives of (36) may be computed for use in (32) as well.

The proportional and derivative gains are set to $\boldsymbol{K}_p = \mathrm{diag}(10^4, 10^4)$, $\boldsymbol{K}_d = \mathrm{diag}(200, 200)$ for a critically damped response, and $k_\omega = 0.5$. The resulting error evolution is shown in Figure 3 for both longitudinal velocity and yaw rate.

Both outputs are successfully controlled to zero error after an initial transient in the longitudinal velocity error. This transient results from a step increase in the desired longitudinal acceleration at the initial time. However, the error is driven back to zero exponentially. The yaw rate error and its derivatives are zero for all time.

Figure 4 shows a comparison of the vehicle yaw rate under control to that of a vehicle with a constant torque of -10 Nm at each wheel (chosen to achieve the same 0.2 m/s^2 longitudinal acceleration) and identical steering input. Here the success of the control is apparent as the uncontrolled vehicle achieves far less yaw rate than its controlled counterpart.

No effects of zero dynamic instabilities were observed, since all signals remained bounded.

V. Conclusions

In this paper, a new vehicle model has been presented. It includes an extended version of the LuGre friction model with terms arising from rotational motion, and an algebraic method of solving for normal force.

An approximation to the relative velocity norm is employed to achieve a sufficiently smooth design model. A reduced output set of longitudinal velocity and yaw rate was chosen to avoid a relative degree singularity.

The design of a controller using the approximate vehicle model for IOL has been presented. Control was implemented in simulation for combined speed and yaw rate control.

The success of the control was limited by the need to keep the frictional forces small to preserve relative degree, requiring less aggressive desired trajectories. This problem requires future work to design approximate IOL controllers that will function for all forces despite relative degree singularities.

References

[1] E. Chowanietz, "Automobile electronics in the 1990s; part2: Chassis electronics," *Electronics & Communication Engineering Journal*, pp. 53–58, April 1995.

[2] A. D. Rodic and M. Vukobratovic, "Contribution to the integrated control synthesis of road vehicles," *IEEE Trans. Contr. Syst. Technol.*, vol. 7, no. 1, pp. 64–78, January 1999.

[3] E. Esmailzadeh, A. Goodarzi, and G. Vossoughi, "Optimal yaw moment control law for improved vehicle handling," *Mechatronics*, vol. 13, no. 7, pp. 659–675, 2003.

[4] H. B. Pacejka and E. Bakker, "The magic formula tyre model," *Vehicle System Dynamics*, vol. 21, no. Supplement, pp. 1–18, 1993.

[5] C. Canudas de Wit, H. Olsson, K. J. Astrom, and P. Lischinsky, "A new model for control of systems with friction," *IEEE Trans. Automat. Contr.*, vol. 40, no. 3, pp. 419–425, March 1995.

[6] C. Canudas de Wit and P. Tsiotras, "Dynamic tire friction models for vehicle traction control," in *Proceedings of the 38th Conference on Decision and Control*, Phoenix, Arizona, December 1999, pp. 3746–3751.

[7] C. Canudas de Wit, P. Tsiotras, E. Velenis, M. Basset, and G. Gissinger, "Dynamic friction models for road/tire longitudinal interaction," *Vehicle System Dynamics*, vol. 39, no. 3, pp. 189–226, 2003.

[8] J. Deur, "A dynamic tire friction model for combined longitudinal and lateral motion," in *Proceedings of 2001 ASME International Mechanical Engineering Congress and Exposition*, New York, NY, 2001, pp. 229–236.

[9] J. H. Ginsberg, *Advanced Engineering Dynamics*, 2nd ed. Cambridge: Cambridge University Press, 1998.

[10] M. G. Villella, "Nonlinear modeling and control of automobiles with dynamic wheel-road friction and wheel torque inputs," Master's thesis, Georgia Institute of Technology, Atlanta, GA, April 2004.